Welding in the World
https://doi.org/10.1007/s40194-025-02220-1

RESEARCH PAPER

Elemental distribution at diffusion bonding interface of FeAlSi thermoelectric material and Cu

Susumu Meguro[1] · Yoshiki Takagiwa[1] · Takashi Kimura[1] · Takanobu Hiroto[1] · Terumi Nakamura[1]

Received: 25 April 2024 / Accepted: 17 October 2025

Abstract
Thermoelectric generation is a promising technology for the realization of a carbon–neutral society. Many kinds of semiconductors are developed as high-efficiency thermoelectric materials. For example, some types of silicide semiconductors consisting of widely available low-cost elements are known to be promising materials. Among them, FeAlSi thermoelectric (FAST) material is a newly developed derivative of iron-silicide material that consists of commonly available non-toxic elements. This material has an excellent Seebeck coefficient up to temperatures of 500 K. With thermoelectric device fabrication, soldering is mainly used to connect FAST material and metal electrodes. However, this connection is unstable in a medium temperature range because the solder melts. Therefore, we investigated the diffusion bonding of FAST material and copper plate, which is stable in a medium temperature range. In this study, we determine the bonding temperature range that allows successful bonding. Furthermore, the elemental distribution at the bonding interface was investigated using EPMA. The mutual diffusion of Al and Cu is dominant in the diffusion bonding process. Furthermore, the crystalline phases of the bonded joint area are investigated using X-ray diffraction. The spectra show that the Fe-Si and Cu-Al phases were precipitated in the Cu-diffused area of the FAST material. These results show that the mutual diffusion and eutectoid reaction of Cu and Al contribute to the diffusion bonding process.

Keywords FeAlSi · Cu · Diffusion bonding · EPMA · X-ray diffraction · Eutectoid reaction

1 Introduction

Thermoelectric generation is a promising technology for the realization of a carbon–neutral society. It is a phenomenon whereby thermal energy is directly exchanged for electrical energy. In addition, thermoelectric generation occurs when a temperature gradient is applied between two connections in an electric circuit consisting of different kinds of material. In this case, the efficiency of the thermoelectric generation is evaluated by a figure of merit ZT, which is given by the following equation: $ZT = S^2\sigma\Delta T/\kappa$. Here, S is the relative Seebeck coefficient, σ is the electrical conductivity, ΔT is the temperature gradient and κ is the thermal conductivity.

This equation shows that a high electrical conductivity and a low thermal conductivity are necessary if we are to increase the ZT. As materials that satisfy these conditions, bismuth telluride (Bi_2Te_3) semiconductor and derivative materials have been continuously developed since the 1950s [1, 2]. In contrast, Bi_2Te_3 has several serious issues, such as high toxicity and a decrease in the Seebeck coefficient at certain temperatures. As a result, many materials have been developed to overcome these issues. For example, some kinds of silicide semiconductors that consist of low-cost and nontoxic ubiquitous elements have been developed [3]. Iron silicides and derivative semiconductor materials have been investigated in terms of their various properties [4, 5]. In this study, we focused on an iron aluminum silicide (Fe-Al-Si) thermoelectric material, called "FAST" material [6–11]. This material is a derivative of iron silicide. Furthermore, the Seebeck coefficient remains at a certain high value up to 500 K in the medium temperature range, and the p-n conduction type is controllable by controlling the chemical composition of Fe, Al, and Si without dopants [7].

Recommended for publication by Commission IX - Behaviour of Metals Subjected to Welding

✉ Susumu Meguro
MEGURO.Susumu@nims.go.jp

[1] National Institute for Materials Science, Tsukuba, Ibaraki 305-0047, Japan

Published online: 17 November 2025

With thermoelectric device fabrication using FAST material, soldering is used to connect the FAST material with a metal electrode [10]. However, this connection is not stable in the 500 K medium temperature range because the solder melts. Therefore, the aim of this study is to investigate the diffusion bonding of the FAST material and copper electrode plate to overcome this issue. Diffusion bonding is a kind of solid-state bonding that connects materials directly without solder. In recent research into the diffusion bonding of dissimilar materials containing Cu and Al, some interesting characterization studies have been reported. These studies include the enhancement of functional properties using the reaction between elements [12], a detailed investigation of an Al-Cu composite microstructure [13], the improvement of performance by using brazing [14], and the improvement of diamond/Cu diffusion bonding with a Ti interlayer [15]. Therefore, when FAST material and copper are combined, we can expect a complicated structure at the bonding interface. Therefore, we investigated the element distribution and undertook a quantitative analysis at the bonding interface using EPMA. Furthermore, X-ray diffraction is carried out to determine the kinds of crystalline phases around the bonding interface. Using these results, we can expect to determine the behavior of the elements and the diffusion bonding mechanism in detail.

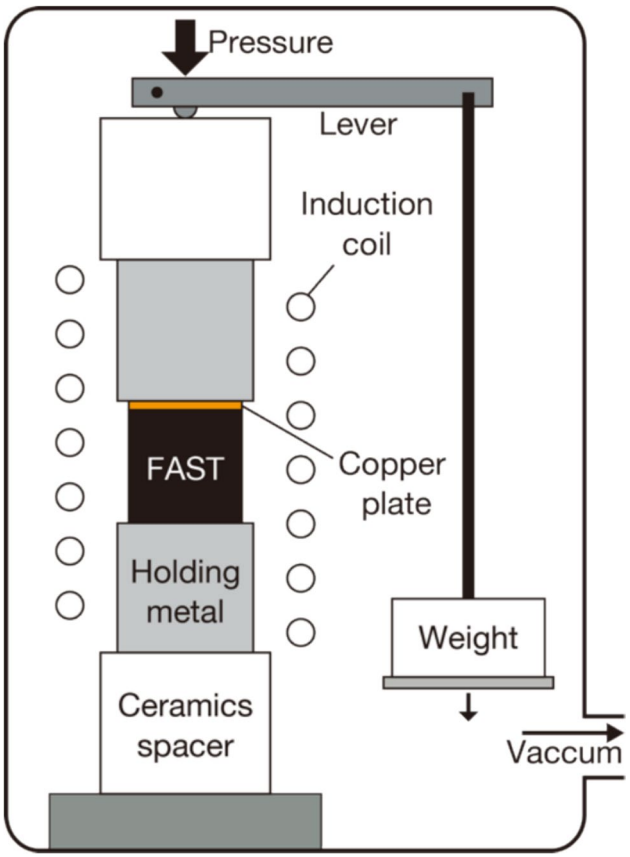

Fig. 1 Schematic view of diffusion bonding

2 Experimental procedure

2.1 Test materials

In this study, FeAiSi (FAST) semiconductor thermoelectric material and oxygen-free copper plate were prepared as test materials. The composition of the FAST material is n-type $Fe_{0.38}Al_{0.24}Si_{0.38}$, which was obtained by machine learning [9]. In addition, this material is chemically stable up to at least 973 K [8]. A powder consisting of a mixture of iron, aluminum and silicon was hot-pressed and then cut to a diameter of 10 mm and a length of 10 mm. Moreover, the circular surface of the FAST material was mirror-polished and then subjected to diffusion bonding. Additionally, 99.96% grade oxygen-free and 0.3-mm-thick copper plates were cut to 15×12 mm and then also subjected to diffusion bonding.

2.2 Diffusion bonding

In this study, we selected diffusion bonding to obtain a direct bonded joint between the FAST material and a copper plate. This method involves solid-state bonding that depends on the diffusion of atoms and creep deformation of materials at the bonding interface. Therefore, no solder is needed to obtain joints. Figure 1 shows a schematic view of the diffusion bonding experiment. The FAST material was heated by thermal conduction from stainless steel holding metal chips because the electrical resistivity of the semiconductor material is too high for the use of RF induction heating. The RF frequency is 40 kHz, which is expected to increase the temperature uniformity in the horizontal direction of the figure. Furthermore, the bonding temperatures were 973 K, 1023 K, 1073 K, 1123 K, and 1173 K. The bonding period was 1800s. After bonding, the specimen including a bonded joint was cooled in the furnace to room temperature without temperature control. In addition, the loading pressure on the materials was 5.1 MPa, which we realized by using a 3-kg weight and lever with a 10:1 ratio. The vacuum in the chamber was kept at less than 10^{-4} Pa during the bonding and cooling process to avoid any oxidization of the materials. Furthermore, the diffusion bonded joint specimens were cut normal to the bonding interface and subjected to macroscale optical observation and microscale elemental analysis.

2.3 Elemental analysis

Line profile, element mapping and quantitative analyses were carried out using EPMA. From these analyses, we obtained information about the diffusion length, two-dimensional distribution of elements and composition of precipitated phases. For the element mapping analysis, we employed the EPMA scatter diagram method. This method determines the composition of precipitates at the bonding interface using the X-ray intensity profile of each element [16]. The accelerating voltage was 15 kV in the line analysis, mapping and most of the quantitative analysis. In addition, for quantitative analysis in a detailed structure, we used an accelerating voltage of 10 kV to improve spatial resolution.

2.4 X-ray diffraction

X-ray diffraction was carried out to identify crystalline phases of precipitates around a bonded joint. This method determines composites and alloys that are precipitated during diffusion bonding.

A micro-focus X-ray diffraction experiment with Cu Kα radiation, which was generated by a Cu-rotator anode with an operating voltage and current of 45 kV and 200 mA, respectively, was performed using an X-ray diffractometer, SmartLab (Rigaku Co. Ltd., Tokyo, Japan), equipped with a HyPix-3000-pixel array detector. A micro-X-ray beam with a 200-μm diameter, which is comparable to the diffusion area, was shaped using a collimator, and the camera was set at a distance of 150 mm.

3 Results and discussion

3.1 Diffusion bonding of FeAlSi (FAST) semiconductor material and copper plate

The diffusion bonding of the FeAlSi (FAST) semiconductor material and copper plate was carried out at bonding temperatures of 973, 1023, 1073, 1123, and 1173 K. Table 1 shows the shapes of the joints and optical images of the cross sections. While cutting cross sections of the joints, the FAST material peeled from the copper plate in the specimen fabricated with a 973 K bonding temperature. On the other hand, at bonding temperatures of 1023 K and 1073 K, diffusion bonding appeared to be successful. Furthermore, cracks were observed in the FAST material. The large crack at the interface of copper and FAST material in the specimen of 973 K bonding temperature is expected to be an unbonded area. On the other hand, the cracks in the FAST material area of the specimens are expected to be generated after diffusion bonding by the difference between the thermal expansion of copper and the FAST material. However, the optical images of the cross-section show that some of the elements in the FAST material or copper can be expected to diffuse across the bonding interface.

Table 1 Overview of specimen and optical image of bonding interface

Bonding temperature	973K	1023K	1073K	1123K	1173K
Side view	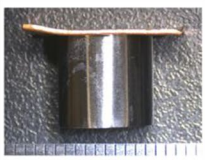	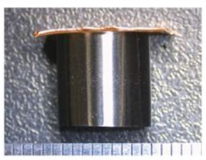	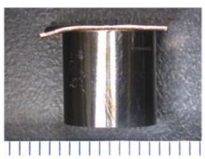	No photo	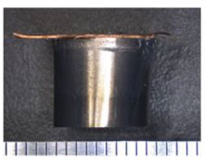
Top view	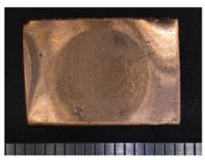	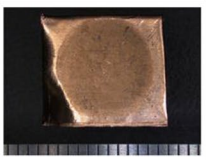	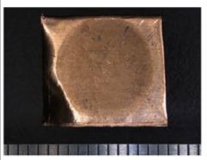	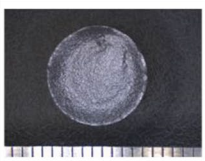	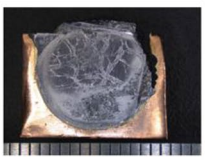
Optical image of cross section	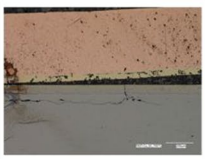	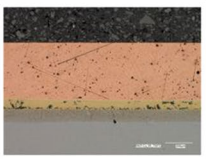	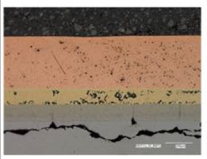	No photo	No photo
State	Peeling at bonding interface	Successful bonding Crack in FeAlSi	Successful bonding Crack in FeAlSi	Fusion of Cu	Fusion of Cu

Moreover, the copper plate disappeared at bonding temperatures of 1123 K and 1173 K. In these cases, the bonding temperature was above the eutectic point of 1076 K for copper and silicon [17]. Therefore, the copper was expected to fuse with the silicon and disappear. These results indicate that the diffusion bonding temperature of FAST material and the copper plate should be below the eutectic point of copper and silicon.

3.2 Line analysis at the bonding interface

Diffusion bonding experiments revealed diffusion layers at the cross section of the optical images below the 1073 K bonding temperature. However, information about the diffused elements across the bonding interface remains unclear. Therefore, we carried out a line analysis using EPMA to determine the kinds of elements and the diffusion length of each element.

Figure 2 shows a composition image and the line analysis scanning position at the bonding interface of the 1073 K bonding temperature specimen. This image is divided into four areas according to brightness. The topmost and bottommost areas are copper plate base material and FAST material, respectively. Furthermore, the middle two areas both seem to be diffused across the bonding interface. In this study, we must identify the diffusion elements if we are to understand the joining process. For these reasons, the line analysis position is set across all areas in the image.

Figure 3 shows the results of the line analysis of the position that is shown in Fig. 2. In this case, Al in the FAST material

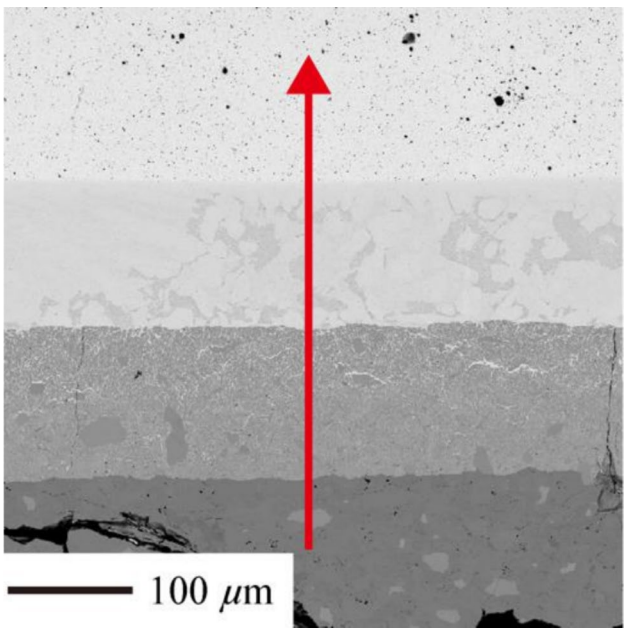

Fig. 2 EPMA composition image and line analysis position of FAST/Cu diffusion bonding interface (bonding temperature 1073 K)

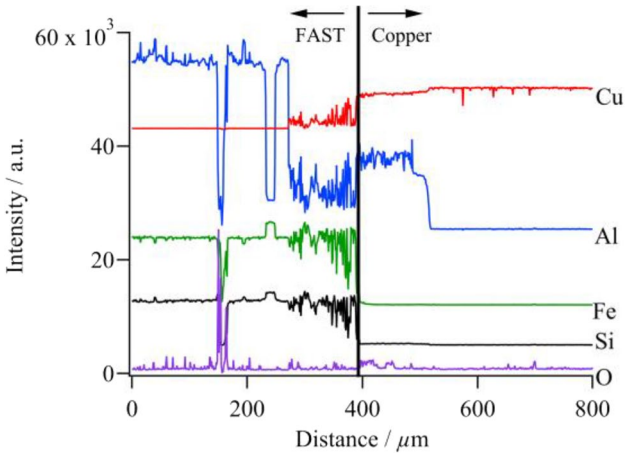

Fig. 3 Line profile across FAST/Cu diffusion bonding interface (bonding temperature 1073 K)

and Cu diffused across the bonding interface. However, the diffusion of Fe and Si into the copper plate was not confirmed. Moreover, similar line profiles were observed at the interface of the specimens with bonding temperatures of 973 K and 1023 K. Figures 4 and 5 show the Al and Cu intensity profiles across the bonding interface of the specimens with bonding temperatures of 973 K, 1023 K, and 1073 K. The diffusion length of Al into the copper plate increased as the bonding temperature increased. Table 2 shows the diffusion lengths. In this study, we performed the line analysis on three lines at different places on the specimen. These values are the averages of the measured lengths. The relationships between the diffusion length L, diffusion coefficient D, and activation energy Q are described by the following equations.

$$L = 2\sqrt{Dt} \tag{1}$$

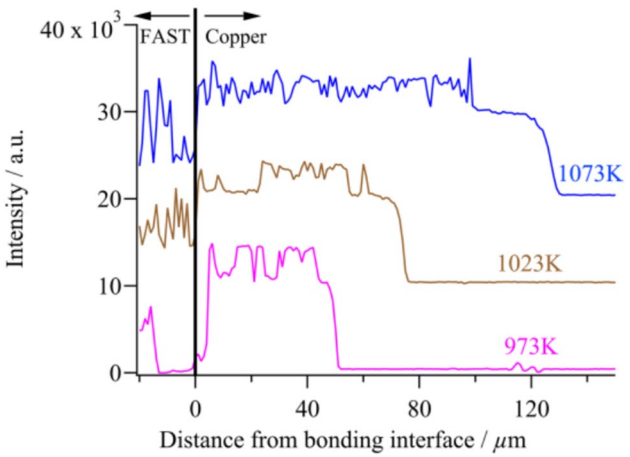

Fig. 4 Al intensity profile across bonding interface

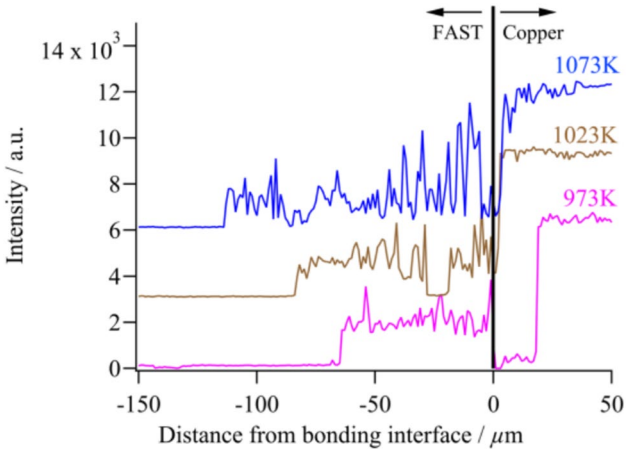

Fig. 5 Cu intensity profile across bonding interface

Table 2 Diffusion length of Al into copper plate and Cu into FAST material

Bonding temperature/K	973	1023	1073
Al diffusion length L/μm	51	75	121
Cu diffusion length L/μm	63	87	122

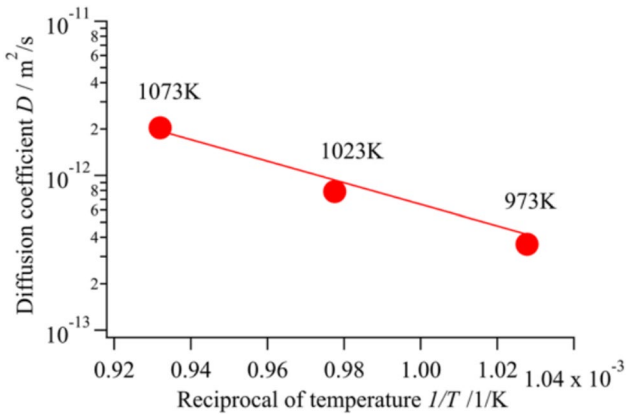

Fig. 6 Arrhenius plot for diffusion coefficient of Al from FAST material to copper plate

$$D = L^2/4t = D_0\mathrm{Exp}(-Q/RT) \quad (2)$$

Here, the t value was fixed at 1800s. D_0 is the diffusion constant, Q is the activation energy, R is the gas constant, and T is the absolute temperature.

Figure 6 shows an Arrhenius plot for the diffusion coefficient of Al from the FAST material to the copper plate. From the plots, D_0 and Q in Eq. (2) were approximated by the following values.

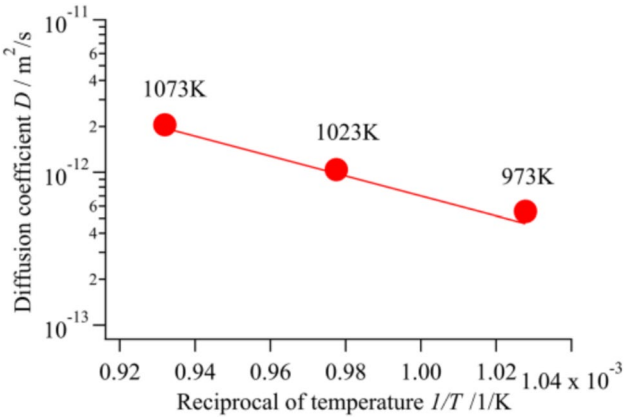

Fig. 7 Arrhenius plot for diffusion coefficient of Cu from copper plate to FAST material

$$D_0 = 3.97 \times 10^{-5}\mathrm{m}^2/\mathrm{s}$$

$$Q = 150\ \mathrm{kJ/mol}$$

Furthermore, Fig. 7 shows an Arrhenius plot for the diffusion coefficient of Cu from the copper plate to the FAST material. D_0 and Q in Eq. (2) were approximated by the following values.

$$D_0 = 6.52 \times 10^{-7}\mathrm{m}^2/\mathrm{s}$$

$$Q = 113\ \mathrm{kJ/mol}$$

3.3 Element mapping at the bonding interface

According to the results of the line analysis reported in the previous section, Cu and Al can be expected to contribute to diffusion bonding. Table 3 shows EPMA mapping images of the composition (CP), Cu, Al, Fe, Si, and O at the bonding interface. The accelerating voltage was 15 kV. The diffusion area of Cu and Al across the bonding interface increased as the bonding temperature increased. These images show the precipitation of some elements. Therefore, we carried out the EPMA scatter diagram method for more detailed phase mapping. In this study, the composition of each phase was estimated using the X-ray intensity correlation of each element. Table 4 shows phase mapping images of the FAST/copper plate bonding interface obtained using the EPMA scatter diagram method. Different compositions of Cu-Al intermetallic compounds were observed in the Al diffusion area of the copper plate. In addition, the structure of the Cu diffusion area in the FAST material was complicated. Fe-Si precipitation occurred not only in the Cu diffused area but also in the base material. Moreover, multiple phases were

Table 3 EPMA mapping images of the composition (CP), Cu, Al, Fe, Si, and O in FAST/copper plate bonding interface (bonding temperature 973 K, 1023 K, and 1073 K)

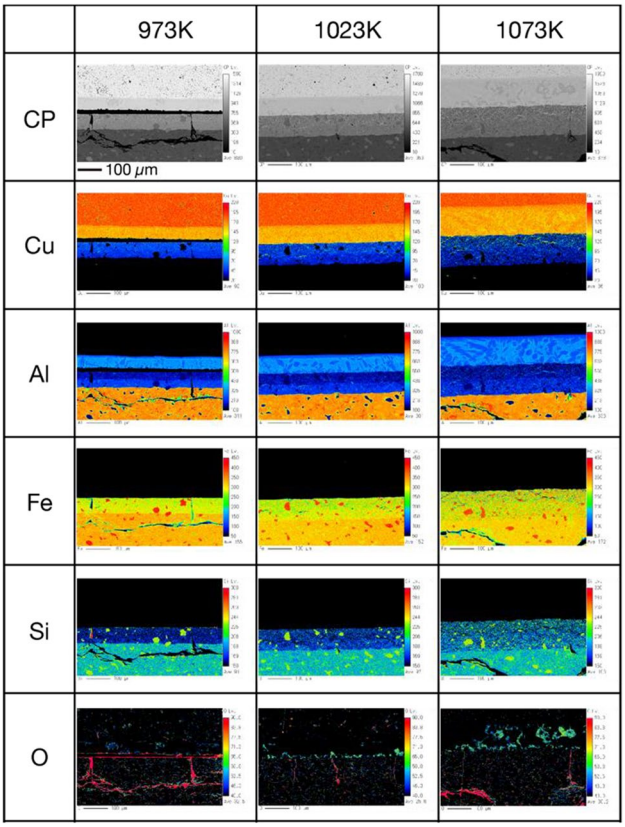

expected to be precipitated in the Cu diffusion area in the FAST material.

To determine the composition of the phases, we undertook a quantitative analysis at several typical points at the bonding interface. Figure 8 shows the quantitative analysis points at the bonding interface of the specimen with a 1073 K bonding temperature. The accelerating voltage was 15 kV. The quantitative values are shown in Table 5. The possible phase was determined using X-ray diffraction, which is described in a subsequent section.

In the Al diffusion area of the copper plate, the Cu-Al phase precipitates at points 3 and 4. Moreover, the Al concentrations at points 1 and 2 in the surrounding area were approximately within the solid solution limit [17]. From the results, the structure of the Al diffusion area was estimated to be a eutectoid microstructure including the Al solid solution phase of Cu and a precipitate of Cu-Al composite.

In the Cu diffusion area in the FAST material, relatively large amounts of precipitation of up to 20 μm were observed. From a quantitative analysis at points 5 and 6 in this area, the precipitation was estimated to be FeSi. Moreover, a similar precipitation was observed in the base material area (points 9 and 10). Here, the FeSi in the base material area was estimated to be generated by a eutectoid reaction during FAST material fabrication before diffusion bonding [11].

Another precipitation was observed in the Cu diffusion area of the FAST material. This is part of the lamellar structure and has a similar composition to Cu-Al (points 11 and 12). In this study, all the bonding temperatures were above the eutectoid point of Cu and Cu_3Al (840 K) [18]. Therefore, we estimated that the structure consists of pro-eutectoid FeSi and a lamellar structure that contains Cu-Al precipitation. Moreover, this lamellar structure was observed only in the Cu diffusion area of the FAST material. It is possible that Fe and Si caused the eutectoid reaction in the area during the diffusion bonding process.

To determine the quantitative values in the lamellar structure in detail, a further analysis was carried out by reducing the accelerating voltage to 10 kV. Figure 9 shows a magnified view of the quantitative analysis points at the bonding interface of the specimen with a 1073 K bonding temperature. The island-like area was expected to be the FeSi phase that exists in the base material. Moreover, in the precipitate phase in the lamellar structure (point 14), we can expect to observe the Cu_3Al phase, which is generated by a eutectoid reaction of Al in the FAST material and Cu. The matrix of the lamellar structure is expected to exhibit the FeSi phase (points 13, 15, and 16).

Table 4 EPMA phase mapping images at FAST/copper plate bonding interface (bonding temperatures 973 K, 1023 K, and 1073 K)

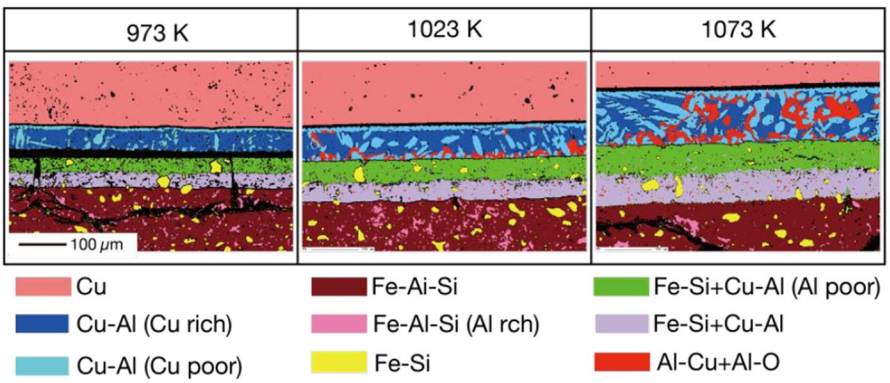

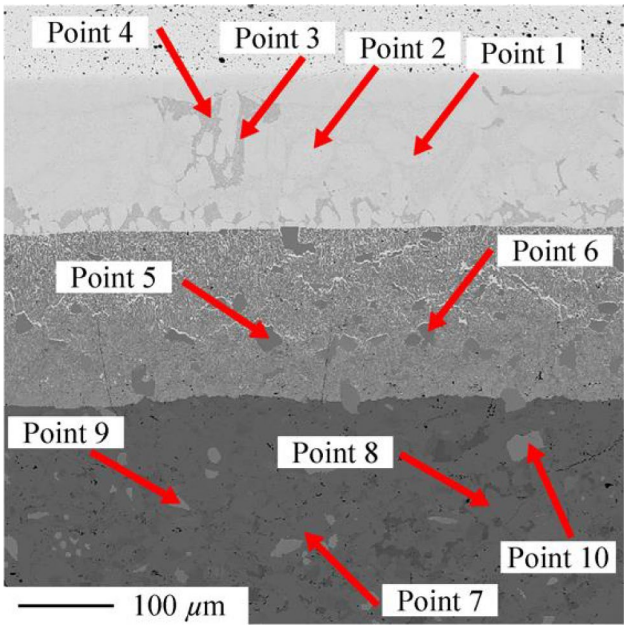

(a) Overall image

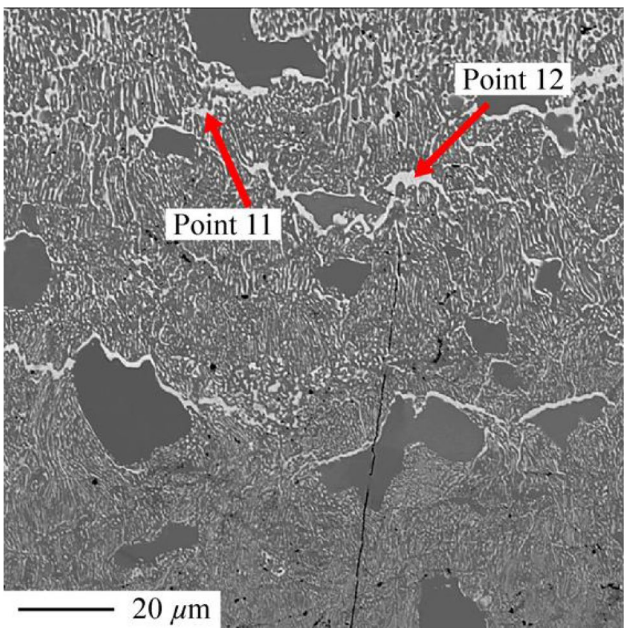

(b) Magnified image near point 5

Fig. 8 Quantitative analysis points at bonding interface of 1073 K bonding temperature specimen. **a** Overall image; **b** magnified image near point 5

3.4 X-ray diffraction analysis (Supplementary material)

In the previous section, the chemical composition of each precipitate around the bonded joint was determined. Furthermore, X-ray diffraction (XRD) analysis was carried out to obtain information about the crystal structure and determine the possible crystalline phase of the precipitates. Figure 10 shows the XRD spectrum of the FAST area, the Cu diffusion area in FAST, and the Al diffusion area in copper. The diffraction spectrum of the FAST material shows peaks of $Fe_3Al_2Si_3$ (τ1). This result agrees with those of previous studies [11, 19]. In the Cu diffusion area in FAST, this spectrum shows that the ε-FeSi phase was generated in addition to $Fe_3Al_2Si_3$. No other peaks were identified in this spectrum because the peaks of them were expected to appear extremely close to the peaks of $Fe_3Al_2Si_3$ and ε-FeSi. Moreover, the spectrum obtained from the Al diffusion copper area shows the Cu, Cu_3Al, and γ-Cu_9Al_4 base material of the plate. Here, the Cu_3Al phase appears at high temperature. However, the bonding process is non-equilibrium. Therefore, the high-temperature phase remained until room temperature was reached. These results and estimations are reflected in Table 5. Here, some peaks could not be identified using only diffraction spectra because the peaks from FAST appeared extremely close in diffraction angles to the peaks from other composites. Therefore, the results by EPMA were used to identify them.

These results show that the mutual diffusion of Al and Cu triggered a eutectoid reaction in the diffusion area of the bonded joint and enhanced the bonding process.

Table 5 Quantitative analysis value near FAST/Cu bonding interface and estimated phase

Point	Cu	Fe	Al	Si	Possible phase
1	81.0	0.2	17.5	1.3	Cu
2	80.3	0.1	18.2	1.4	Cu
3	72.3	0.0	25.9	1.8	Cu3Al + Cu9Al4
4	71.4	0.1	26.6	1.9	Cu3Al + Cu9Al4
5	0.2	49.5	5.2	45.1	e-FeSi
6	0.2	49.5	5.1	45.1	e-FeSi
7	< 0.1	37.4	26.1	36.5	FAST
8	< 0.1	37.2	26.8	35.9	FAST
9	< 0.1	49.4	5.2	45.4	e-FeSi
10	< 0.1	49.6	5.1	45.2	e-FeSi
11	74.0	4.1	20.9	1.0	Cu3Al
12	75.3	5.0	18.5	1.2	Cu3Al
13	1.3	45.4	2.3	50.9	e-FeSi
14	72.0	3.0	24.1	0.8	Cu3Al
15	0.9	49.5	3.2	46.4	e-FeSi
16	0.9	48.3	2.9	47.9	e-FeSi

4 Conclusions

The diffusion bonding of FeAlSi (FAST) thermoelectric material and copper plate was successful. Moreover, the following results were obtained with elemental analysis using EPMA at the diffusion bonding interface.

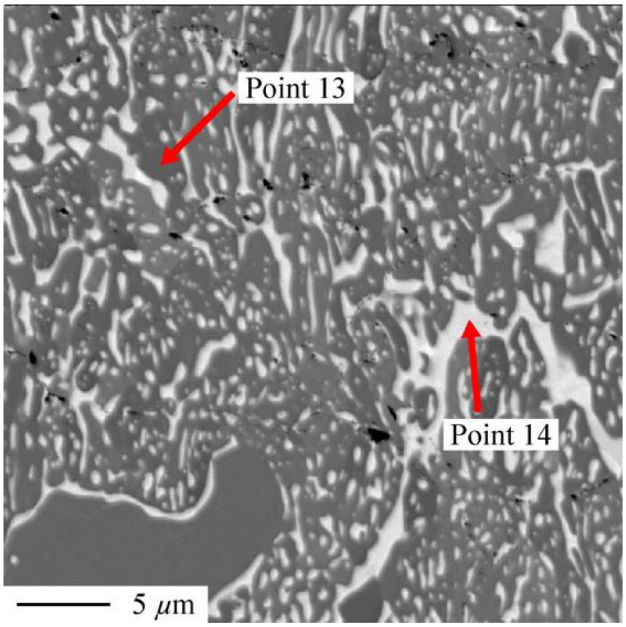

(a) Near bonding interface

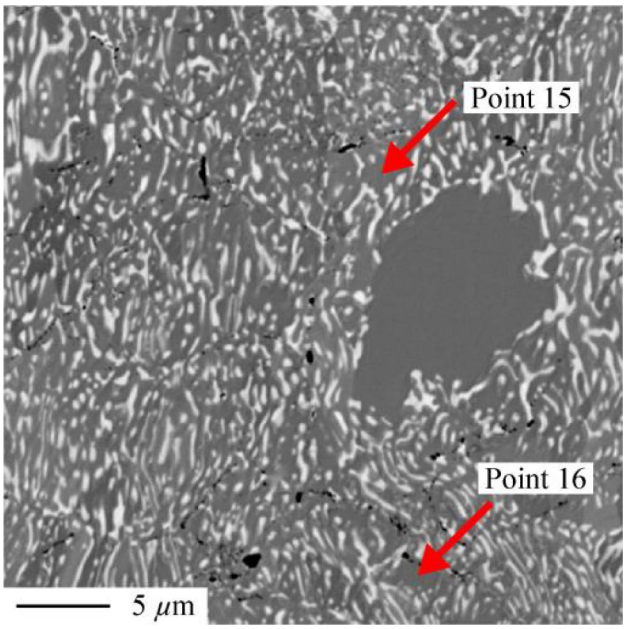

(b) Near base material

Fig. 9 Quantitative analysis points at bonding interface of 1073 K bonding temperature specimen (10 kV). **a** Near bonding interface; **b** near base material

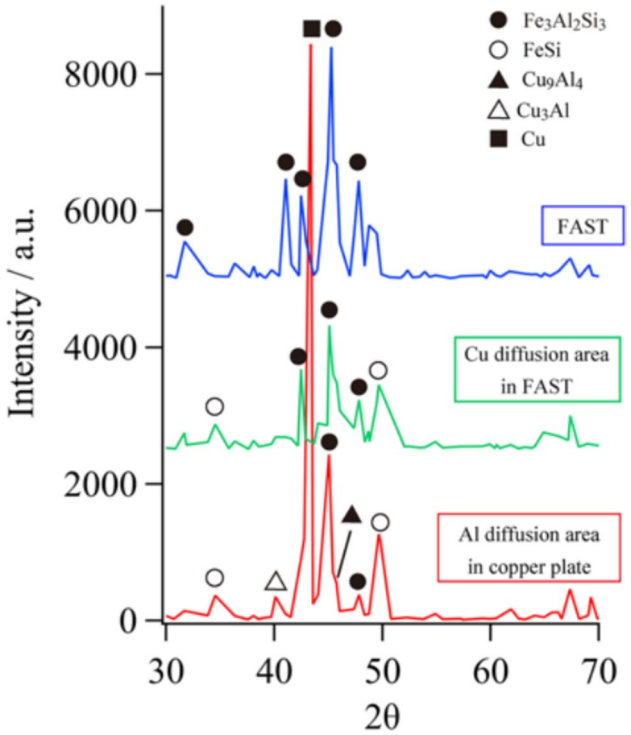

Fig. 10 X-ray diffraction spectra in FAST/Cu diffusion bonded intnt (1073K bonding temperature)

1. Diffusion bonding occurs at bonding temperatures ranging from 973 to 1073 K. Moreover, the diffusion bonding temperature should be below the eutectic point of Cu and Si.
2. Line analysis and element mapping using EPMA revealed that the mutual diffusion of Al and Cu is dominant in the diffusion bonding process. Moreover, the diffusion constant and activation energy of these elements were obtained.
3. EPMA quantitative analysis, scatter diagram method, and X-ray diffraction revealed Cu_3Al-based precipitation and an ε-FeSi matrix in the lamellar microstructure of the Cu diffusion area of the FAST material. Furthermore, the Cu-Al solid solution, γ-Cu_9Al_4 and Cu_3Al phases were observed in copper material. It is possible that the eutectoid reaction of Cu and Al enhances the diffusion bonding process of FAST material and copper.

Acknowledgements The authors thank Koji Nakazato of the Materials Forming Unit in the National Institute for Materials Science (NIMS) for preparing the EPMA and X-ray diffraction specimens.

Author contributions S. Meguro performed the diffusion bonding, evaluated the specimens and wrote the manuscript. Y. Takagawa proposed the chemical composition of FAST material and distributed the material. T. Kimura performed the characterizations of specimens using EPMA. T. Hiroto performed the characterizations of specimens using X-ray diffraction. T. Nakamura advised on the whole manuscript. All authors have read and agreed to the manuscript.

Funding A part of this study was supported by Mitsuaki Nishio of the Surface and Bulk Analysis Unit in the National Institute for Materials Science (NIMS) for EPMA analysis.

Data availability Not applicable.

Declarations

Competing interests The authors declare no competing interests.

References

1. Goldsmid HJ (2014) Bismuth telluride and its alloys as materials for thermoelectric generation. Materials 7:2577–2592. https://doi.org/10.3390/ma7042577
2. Wei J, Yang L, Ma Z, Song P, Zhang M, Ma J, Yang F, Wang X (2020) Review of current high-ZT thermoelectric materials. J Mater Sci 55:12642–12704. https://doi.org/10.1007/s10853-020-04949-0
3. Nozariasbmarz A et al (2017) Thermoelectric silicides: a review. Jpn J Appl Phys 56:05DA04. https://doi.org/10.7567/JJAP.56.05DA04
4. Heinrich A et al (2001) Thermoelectric properties of β-FeSi2 single crystals and polycrystalline β-FeSi2+x thin films. Thin Solid Films 381:287–295. https://doi.org/10.1016/S0040-6090(00)01758-2
5. Nishida I (1973) Study of semiconductor-to-metal transition in Mn-doped FeSi2. Phys Rev B 7:2710–2713. https://doi.org/10.1103/PhysRevB.7.2710
6. Takagiwa Y, Isoda Y, Goto M, Shinohara Y (2018) Electronic structure and thermoelectric properties of narrow-band-gap intermetallic compound Al2Fe3Si3. J Therm Anal Calorim 131:281–287. https://doi.org/10.1007/s10973-017-6621-9
7. Takagiwa Y, Isoda Y, Goto M, Shinohara Y (2018) Conduction type control and power factor enhancement of the thermoelectric material Al2Fe3Si3. J Phys Chem Solids 118:95–98. https://doi.org/10.1016/j.jpcs.2018.03.003
8. Takagiwa Y, Shinohara Y (2019) A practical appraisal of thermoelectric materials for use in an autonomous power supply. Scr Mater 172:98–104. https://doi.org/10.1016/j.scriptamat.2019.07.022
9. Hou Z, Takagiwa Y, Shinohara Y, Xu Y, Tsuda K (2019) Machine-learning-assisted development and theoretical consideration for the Al2Fe3Si3 thermoelectric material. ACS Appl Mater Interfaces 11:11545–11554. https://doi.org/10.1021/acsami.9b02381
10. Takagiwa Y, Hou Z, Tsuda K, Ikeda T, Kojima H (2021) Fe−Al−Si thermoelectric (FAST) materials and modules: diffusion couple and machine-learning-assisted materials development. ACS Appl Mater Interfaces 13:53346–53354. https://doi.org/10.1021/acsami.1c04583
11. Srinithia AK, Sepehri-Amina H, Takagiwa Y, Hono K (2022) Effect of microstructure on the electrical conductivity of p-type Fe–Al–Si thermoelectric materials. J Alloy Compd 903:163835. https://doi.org/10.1016/j.jallcom.2022.163835
12. Yao F, You G, Zeng S, Lu D, Ming Y (2023) Reaction-tunable diffusion bonding to multilayered Cu mesh/ZK61 Mg foil composites with thermal conductivity and lightweight synergy. J Mater Sci Technol 139:10–22. https://doi.org/10.1016/j.jmst.2022.07.060
13. Wang C, Chen J, Liang S, Shao W, Yang XY (2023) Microstructure evolution and mechanical properties of CuW/Al interface fabricated by infiltration and vacuum hot-pressing diffusion bonding. Vacuum 210:111882. https://doi.org/10.1016/j.vacuum.2023.111882
14. Zhang Y, Guo W, Yin CH, Xu YQ, Mei H, Shao TW, Zhu Y, Zhang HQ (2024) The interlayer self-reinforcement and filler re-optimization achieving multiple collaborative enhancement of the brazed superalloy heterogeneous joint. Mater Sci Eng A 903:146694. https://doi.org/10.1016/j.msea.2024.146694
15. Hu DC, Wang L, Chen L, Feng S, Wang N, Zhou Y (2023) Thermal conduction and strength of diamond-copper composite sandwich obtained by SPS diffusion bonding with Ti interlayer. J Mater Res Technol 26:8806–8812. https://doi.org/10.1016/j.jmrt.2023.09.188
16. Kimura T, Sugisaki T, Nishida K, Ishikawa N, Tanuma S (2004) Analysis of joining boundary between Ni-P electroless plate and solder by EPMA scatter diagram method (I). J Japan Inst Metals 68:8–13
17. Okamoto H (2002) Cu-Si (copper-silicon). J Phase Equilib 23:281–282. https://doi.org/10.1361/105497102770331857
18. Murray J. L, Al-Cu Phase Diagram (1990). ASM alloy phase diagrams database, P. Villars, editor-in-chief; H. Okamoto and K. Cenzual, section editors; http://www.asminternational.org, ASM International, Materials Park, OH, 2016.
19. Marker MCJ, Skolyszewska-Kühberger B, Effenberger HS, Schmetterer C, Richter KW (2011) Phase equilibria and structural investigations in the system Al-Fe-Si. Intermetallics 19:1919–1929. https://doi.org/10.1016/j.intermet.2011.05.003